Proceedings of the ASME 2010 10th Biennial Conference on Engineering Systems Design and Analysis
ESDA2010
July 12-14, 2010, Istanbul, Turkey

ESDA2010-25034

NUMERICAL SIMULATION OF CONE FORMATION IN ELECTROSPRAYING PROCESS

Mohammad Passandideh Fard
Associate Professor, Department of Mechanical Engineering
Ferdowsi University of Mashhad, Iran
mpfard@um.ac.ir

Mortaza Rahimzadeh
Graduate Student, Department of Mechanical Engineering
Ferdowsi University of Mashhad, Iran
Mortaza_rahimzadeh@yahoo.com

Sajad Pooyan
Graduate Student, Department of Mechanical Engineering
Ferdowsi University of Mashhad, Iran
Sajad.pooyan@gmail.com

ABSTRACT

A numerical model is developed to study the transient behavior of a liquid jet leaving a capillary tube under an electrostatic field. The surface profile of the deforming jet is defined using the Volume-of-Fluid (VOF) scheme and the advection of the liquid free-surface is performed using Youngs' algorithm. Surface tension force is treated as a body force acting on the free-surface using continuum surface force (CSF) method. To calculate the effect of the electric field on the shape of the free-surface, the electrostatic potential is solved first. Next, the surface density of the electric charge and the electric field intensity are computed, and then the electric force is calculated. Liquid is assumed to be a perfect conductor, thus the electric force only acts on the liquid free-surface and is treated similar to that of surface tension using the CSF method. The developed model is validated by a comparison between the calculated results and measurements for an electrowetting scenario for which experimental results are available in the literature.

INTRODUCTION

Electrostatic atomization, also called Electrospray, is a well known phenomenon in which an electrostatic force elongates the liquid meniscus formed at the outlet of a capillary nozzle to a jet which next disrupts into small droplets by electrical and mechanical forces. Electrospray systems have several advantages over mechanical atomizers. The size of electrospray drops can range from hundreds of micrometers down to several tens of nanometers. The size distribution of the droplets can be nearly monodisperse. Droplet generation and droplet size can be controlled roughly via the control of the flow rate of the liquid and the applied voltage at the capillary nozzle. The fact that the droplets are electrically charged facilitates the control of their motion (including their deflection and focusing) by means of an electric field. Charged droplets are self dispersing in space, also resulting in the absence of droplet coagulation. The deposition efficiency of a charged spray on an object is higher than that of an un-charged spray. This feature can be utilized, for example, in surface coating or thin-film production.

Electrospray has opened new routes to nanotechnology. Electrospray is used for micro and nano-thin-film deposition, micro or nano-particle production, and micro- or nano-capsule formation. Thin films and fine powders are (or potentially could be) used in modern material technologies, microelectronics, and medical technology [1]. In spite of these advantages, this method of atomization has some difficulties to perform. The main difficulty is the existence of many different atomization modes depending on the settings of the process. Jaworek et al. [2] classified ten modes of atomization according to geometrical forms of the meniscus and/or jet. Therefore numerical simulation is an effective method to understand and control the phenomenon.

Many studies contributed to the understanding of the phenomenon by modeling and simulation of the involved processes numerically. Hartman et al. [3] developed a

Lagrangian model to predict droplet size and velocity and compared the results with those of the experiments. They improved a physical model to obtain the shape of the liquid cone and jet; the electric fields inside and outside the cone; and the surface charge density on the liquid surface [4]. In their model, a one-dimensional momentum equation was used to simulate the flow field. Using an analytical model, Hartman et al. [5] found that the jet break-up mechanism depends on the ratio of the normal stress from the electric field to that of the surface tension.

Alfonso et al. [6] modeled electrospray using a hybrid experimental-numerical technique. They proved that the surface charges are always in equilibrium, being the liquid bulk quasi-neutral. They presented a consistent general scaling of all electro-hydro-dynamic (EHD) variables involved which are verified by experiment. Fang et al. [7] used a model similar to that of Hartman et al. [4] but solved axisymmetric flow equations and used an adaptive grid generation scheme. They did not consider the jet break up in their model. Zeng et al. [8] used VOF method to simulate Taylor cone formation. While previous models could only predict the steady shape of the cone-jet, Zeng et al. [8] could capture the transition events as well. However, they did not consider jet break up and droplet formation; they also used a semi conductor liquid in their simulations. Lastow et al. [9] performed a simulation similar to that of Zeng et al. [8], but they studied conductive fluid atomization. They did not consider jet break up and surface tension effects in their model.

As mentioned above, most studies available in the literature focused on the steady state solution of the liquid jet profile under electrostatic field. The transient behavior of the liquid jet deformation, the transient mode, and the corresponding conditions for achieving this mode were not studied. The jet-break up and surface tension effects were also not included. In this paper, we use a VOF scheme to model transient behavior of electrospraying considering surface tension and jet-break up. This work can easily be extended to model other atomization modes such as dripping, microdripping and spindle modes.

MATHEMATICAL MODEL

The configuration of the problem is depicted in **Error! Reference source not found.** and the dimensions of the parts pointed at by alphabetic indexes are cited at the last column of "Table 1".

A conductive liquid jet leaves a capillary nozzle with a constant volume flow rate, $Q = 5\,\mu L/min$. The electric voltage applied between nozzle and counter electrode is $\phi_0 = 2.8\,KV$.

Fluid Flow

The fluid flow is assumed incompressible, axisymmetric, Newtonian and laminar. As the air surrounding the liquid jet is not being forced, it does not significantly the liquid motion. Therefore, the shear stresses at the liquid gas interface are not considered. The mass and momentum conservation equations are as follows:

$$\vec{\nabla}.\vec{V} = 0 \tag{1}$$

$$\frac{\partial \vec{V}}{\partial t} + \vec{\nabla}.(\vec{V}\vec{V}) = -\frac{1}{\rho}\vec{\nabla}p + \frac{1}{\rho}\vec{\nabla}.\vec{\tau} + \vec{g} + \frac{1}{\rho}\overrightarrow{F_b} \tag{2}$$

where $\vec{V}$, p, ρ and $\vec{\tau}$ represent the velocity vector, pressure, the liquid density and the stress tensor respectively; $\vec{g}$ is the gravitational acceleration and $\overrightarrow{F_b}$ is any body force (per unit volume) acting on the fluid. As the fluid is Newtonian the stress tensor is:

$$\vec{\tau} = \mu\left[(\vec{\nabla}\vec{V}) + (\vec{\nabla}\vec{V})^T\right] \tag{3}$$

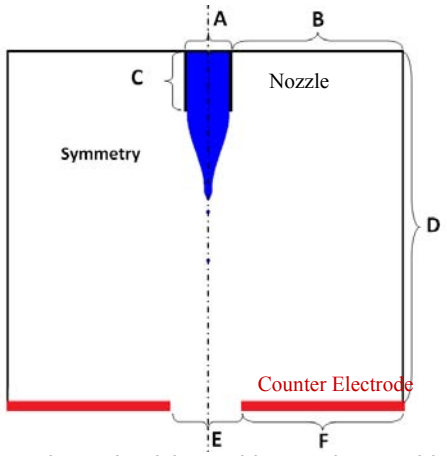

Figure 1: Schematic of the problem under consideration. The electric potential is applied between the nozzle and the counter electrode.

Solving the above equations, the flow field in the computation domain is obtained. The VOF method is then used to advect the free surface location. In this method, a scalar function *f*, called volume fraction, is defined as the fraction of a cell volume occupied by liquid. *f* is assumed to be unity when a cell is fully occupied by the liquid and zero for an empty cell. Cells with f values of $0 < f < 1$ define the location of free surface. The advection equation for volume fraction as

$$\frac{\partial f}{\partial t} + (\vec{V}.\nabla)f = 0 \tag{4}$$

provides the *f* field in each time step.

Electrostatic Force

Along with the hydrodynamic equations presented above, the Laplace equation [10] is solved on the entire domain to calculate the electric potential in every grid cell at each time step:

$$\nabla^2\phi = 0 \tag{5}$$

In addition, the relation between the electric potential and the electric field intensity is known to be:

$$\vec{E} = -\nabla\phi \tag{6}$$

Since the liquid is assumed to be a perfect conductor, the electrostatic force only acts on the liquid free-surface [11]. The electrostatic force per unit area is computed as [12]:

$$\overrightarrow{F_e} = \frac{1}{2}\rho_s\vec{E} \tag{7}$$

where ρ_s is the surface density of the electric charge calculated as:

$$\rho_s = -\varepsilon_{Air}\frac{\partial\phi}{\partial n} = -\varepsilon_{Air}\vec{E}.\hat{n} \tag{8}$$

where $\frac{\partial}{\partial n}$ represents the gradient along the outward normal to the liquid free surface.

Boundary Conditions

A Neumann condition is used for pressure in all domain boundaries ($\frac{\partial p}{\partial n} = 0$). Also, an outflow boundary condition is used for velocity on all boundaries except on solid walls and at the entry of the nozzle where constant velocity is employed. A summary of boundary conditions is mentioned in Table 1.

Table 1: Summary of applied boundary conditions based on the schematic shown in Figure 1.

	Velocity	Pressure	potential	mm
A	$v = {}^{Q}/_{A}$	${}^{\partial P}/_{\partial n}=0$	$\phi = \phi_0$	0.51
B	${}^{\partial u}/_{\partial n}=0$, ${}^{\partial v}/_{\partial n}=0$	${}^{\partial P}/_{\partial n}=0$	${}^{\partial \phi}/_{\partial n}=0$	9.0
C	$u = 0 , v = 0$	${}^{\partial P}/_{\partial n}=0$	$\phi = \phi_0$	5.0
D	${}^{\partial u}/_{\partial n}=0$, ${}^{\partial v}/_{\partial n}=0$	${}^{\partial P}/_{\partial n}=0$	${}^{\partial \phi}/_{\partial n}=0$	15
E	${}^{\partial u}/_{\partial n}=0$, ${}^{\partial v}/_{\partial n}=0$	${}^{\partial P}/_{\partial n}=0$	${}^{\partial \phi}/_{\partial n}=0$	6.0
F	$u = 0 , v = 0$	${}^{\partial P}/_{\partial n}=0$	$\phi = 0$	6.0

As the liquid is assumed a perfect conductor, the electric potential for the points inside the liquid is equal to the applied potential. The liquid used in this study was 50% (v/v) methanol in water with physical properties as listed in Table 2.

Table 2: Physical properties of (50% (v/v) methanol in water)

Density ρ $\left(\frac{Kg}{m^3}\right)$	Viscosity $\mu(Pa.s)$	Surface tension $\gamma\ ({}^{N}/_{m})$	Conductivity ${}^{\mu S}/_{cm}$
894	1.8×10^{-3}	0.0358	3.5

NUMERICAL PROCEDURE

The Youngs algorithm [13] is used for advection of function *f*. This algorithm consists of two steps: an approximate construction of the free surface and the advection of the interface to a new location. First, the interface is reconstructed by locating a line within each interfacial cell utilizing volume fraction of the cell, *f*, and normal vector to the interface. Normal vectors are computed using *f* function gradients in two directions. In the second step, the reconstructed interface and new velocities are used to compute volume fluxes across each cell face in one coordinate direction at a time. Having calculated the advection of the interface in all directions, the final volume fraction field and the new shape of the interface are obtained.

Surface tension is modeled as a volume force acting on fluid elements near the free surface; the method used is the continuum surface force (CSF) model [14] integrated with smoothed values of function f in evaluating free surface curvature [15].

The time discretization of the momentum equation is divided into two steps. First, an interim velocity is computed explicitly from convective, viscous, gravitational, and body forces for a time step Δt. Then, the pressure is calculated implicitly. As momentum cannot be advected more than a grid per time step, the Courant number should be less than one. The same condition is applied for the volume tracking as it can be only advected to the neighboring cells. Further details of the solution procedure of the hydrodynamic equations using VOF method is given elsewhere [15].

The solution of the electrostatic equations in order to obtain the corresponding force distribution on the free surface is explained in details. Some difficulties arise from constant electric potential throughout the main liquid jet. It means that the free surface of the liquid is a Dirichlet condition as the value of the electric potential on free surface is known and set to be that of the nozzle. The deforming liquid interface may have any arbitrary shape that does not necessarily coincide with the edges of the computational cells. To resolve this issue we use five neighboring nodes in different locations with respect to the reconstructed interface to discrete the Laplace equation, Eq. (5), near the free surface. These nodes near the free surface are schematically illustrated in Figure 2.

By employing a non-uniform Cartesian mesh, Eq. (5) may be discretized as follows:

$$\frac{2}{A}\left\{r_R\left(\frac{\phi L_{i+1,j}-\phi C}{\Delta XR_{i,j}+\Delta XL_{i+1,j}}\right) - r_L\left(\frac{\phi C-\phi R_{i-1,j}}{\Delta XR_{i-1,j}+\Delta XL_{i,j}}\right)\right\} + \frac{2}{B}\left\{r_C\left(\frac{\phi B_{i,j+1}-\phi C}{\Delta YT_{i,j}+\Delta YB_{i,j+1}}\right) - r_C\left(\frac{\phi C-\phi T_{i,j-1}}{\Delta YT_{i,j-1}+\Delta YB_{i,j}}\right)\right\} = 0 \quad (9)$$

where:

$$A = \Delta XR_{i-1,j} + \Delta XL_{i,j} + \Delta XR_{i,j} + \Delta XL_{i+1,j}$$
$$B = \Delta YT_{i,j-1} + \Delta YB_{i,j} + \Delta YT_{i,j} + \Delta YB_{i,j+1} \quad (10)$$

and:

$$r_C = r_{i,j}$$
$$r_L = r_C - \frac{\Delta XR_{i-1,j} + \Delta XL_{i,j}}{2}$$
$$r_R = r_C + \frac{\Delta XR_{i,j} + \Delta XL_{i+1,j}}{2} \quad (11)$$

$\Delta XL_{i,j}$, $\Delta XR_{i,j}$, $\Delta YB_{i,j}$ and $\Delta YT_{i,j}$, shown in Figure 2, are parameters computed for each cell near the interface depending on the free surface location. As explained before, a boundary condition needs to be satisfied on the free surface while solving Eq. (5), therefore, the above parameters must be calculated in order to exactly locate the reconstructed free surface profile with respect to the computational grid.

These parameters take different values, depending on the orientation of the interface line in a cell. Nearly ten different arrangements may occur depending on the *f* value and the free surface orientation. One of these arrangements in which the interface line intersects both horizontal edges of the cell is illustrated in Figure 3. For this case, the parameters are:

$$\phi R_{i,j} = \phi_0 \ , \phi L_{i,j} = \phi_0$$
$$\phi \mathrm{T}_{\mathrm{i,j}} = \phi_{\mathrm{i,j}} \ , \phi \mathrm{B}_{\mathrm{i,j}} = \phi_{\mathrm{i,j}}$$
$$\Delta XL_{i,j} = 0 \ , \Delta XR_{i,j} = R$$
$$\Delta YB_{i,j} = \frac{\Delta Y_{i,j}}{2} \ , \Delta YT_{i,j} = \frac{\Delta Y_{i,j}}{2} \quad (12)$$

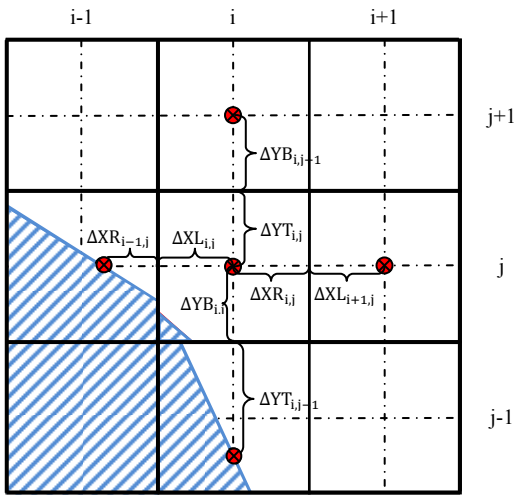

Figure 2: Nodes (red points) used to discrete the Laplace equation in a sample situation. Geometrical parameters appeared in Eqs. (9) and (10) are also illustrated.

ϕR, ϕL, ϕT and ϕB are electric potentials used in the discretization of Eq. (5). If a node selected to discrete the equation lies on the free surface, its value is known and equal to the applied potential ϕ_0, otherwise, it must be calculated.

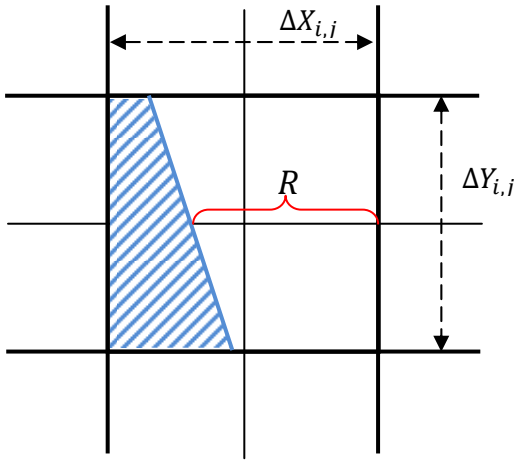

Figure 3: One orientation for the free surface where the interface line intersects both horizontal edges of the cell and one of the symmetry lines.

Electric field intensity

The electric field intensity on the free surface needs to be calculated to obtain the surface density of the electric charge and the electric force acting on the free surface. Again, arbitrary position of the free surface on Cartesian mesh is an issue here. As shown in Figure 4, first we find the midpoint of the approximated interface line in each cell. Then, three directions are considered: the first two being the x and y directions and the third is the direction of the line connecting the centerpoint of reconstructed interface line and the center of (i+2,j+2) cell (pointed out by 'dia' subscript here as shown in Figure 4). Next the derivative of the electric potential is computed on these directions $\left(\frac{\partial \phi}{\partial x}, \frac{\partial \phi}{\partial y}, \frac{\partial \phi}{\partial n_{Dia}}\right)$. As the free surface is a boundary inside the computational domain, we must use directional derivative outward from the fluid interface. As shown in Figure 4 we select three nodes in each direction (nodes specified with red color in Figure 4), and compute the derivatives. These nodes, however, do not lie in the center of cells thus their values are initially unknown; they are calculated by interpolating between the three points. For example to find the electric potential at the red point in cell (i+2,j) of Figure 4, we use three green points as shown in the figure.

Having obtained the above derivatives, we need to calculate the electric field intensity vector by using two of the above derivatives depending on the values of f in the adjacent cells.

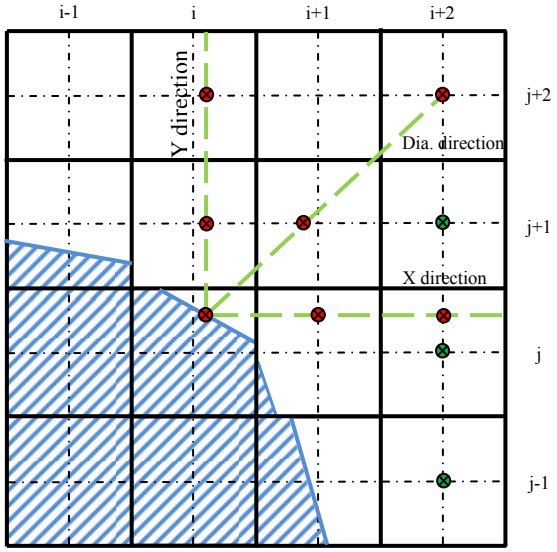

Figure 4: Nodes and directions used for the electric field intensity calculation. First, three green points are used to obtain the electric potential value at each red point. The red points are then used to calculate the potential derivative (Only the three green points used to interpolate the potential value on the red point within cell (i+2,j) are shown in the figure).

MODEL VALIDATION

Solving the Laplace equation for an irregular domain has been reported [16] but its integration with VOF scheme is new in this study. To validate the formulation and the implementation of the numerical scheme, the results are compared with the analytical solutions data.

Consider a solid hemisphere placed on a lower plate of a capacitor **Error! Reference source not found.**. The solid is conductive and has the bottom plate potential. For this case, the method of images can be used to calculate the electric field on the surface as [17]:

$$\left|\vec{E}\right| / \left|\vec{E}_{\infty}\right| = 3\cos\theta \qquad 0 \le \theta \le \pi/2 \tag{13}$$

where θ is the polar angle measured from the apex, as shown in the inset of Figure 6 and $\vec{E}_{\infty}$ is the uniform electric field between plates far from the hemisphere.

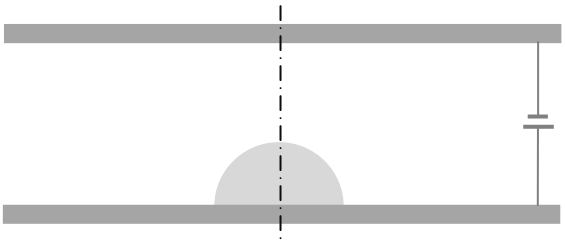

Figure 5: A solid hemisphere placed on a lower plate of a capacitor. The drop is conductive and has the same potential as that of the lower plate.

Figure 6 compares the numerical and analytical electric field magnitudes and their horizontal and vertical components, calculated along the surface (i.e., from the apex to the contact point). The figure shows a good agreement between the numerical results and those of the analytical method.

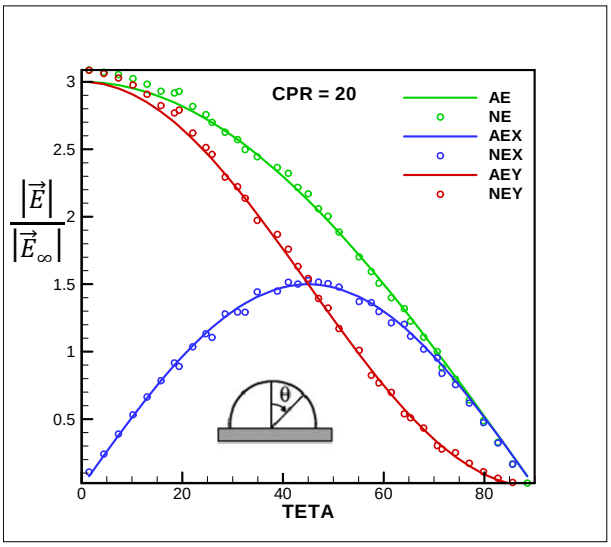

Figure 6: A comparison between analytical and numerical solutions for a hemispherical conductive solid between two conductive plates. There were 20 cells per droplet radius in this simulation (CPR = 20). E, EX and EY denote non-dimensional $|\vec{E}|$, E_x and E_y respectively. The prefix A and N specify the analytical and numerical data, respectively.

NUMERICAL PARAMETERS

Up to this point, the numerical method to simulation the electrostatic field was explained and validated. The main goal of this section is to model the electrostatic atomization process. One of the main issues concerning to numerical simulation of this process is that it needs to deal with different length scales in the solution domain. The largest of them is the length scale related to the spacing between the capillary nozzle and the electrode facing it, this length is from the order of 10^{-2} meter. Another length scale is that of the cone which forms at the outlet of the capillary nozzle and is from the order of 10^{-4} meter. The smallest length scale is associated with the jet departing from the vertex of the cone which is from the order of 10^{-6} meter. The cone shaped part and the jet part or the flow are illustrated in Figure 7. In this work the formation of the cone shaped part is focused on and the jet part is assumed neglidible in simulation due to it's negligible size in comparison with the size of the cone part. This assumption has no significant effect on the cone part and just decreases the accuracy of the solution at the vicinity of the cone vertex.

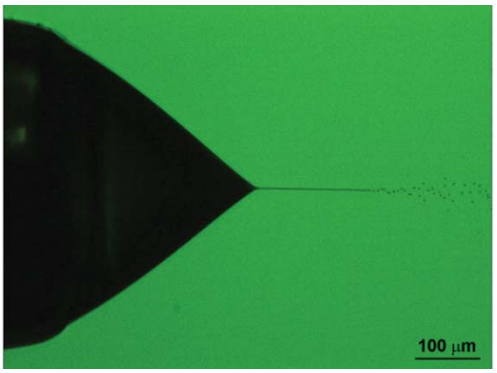

Figure 7: The cone shaped part and the jet departing from the vertex of the cone(length scales are comparable in the image) [18]

In order to manage the problem of different length scales in the domain we divide the solution domain into two zones:

1. The zone in which both hydrodynamic and electrostatic equations are solved (this zone is referred to as zone 1).
2. The zone in which just electrostatic equations are solved (this zone is referred to as zone 2).

These two zones are illustrated in Figure 8. The zone defined by solid black color at the centre of the domain is the zone 1 and the rest of the domain is treated as zone 2.

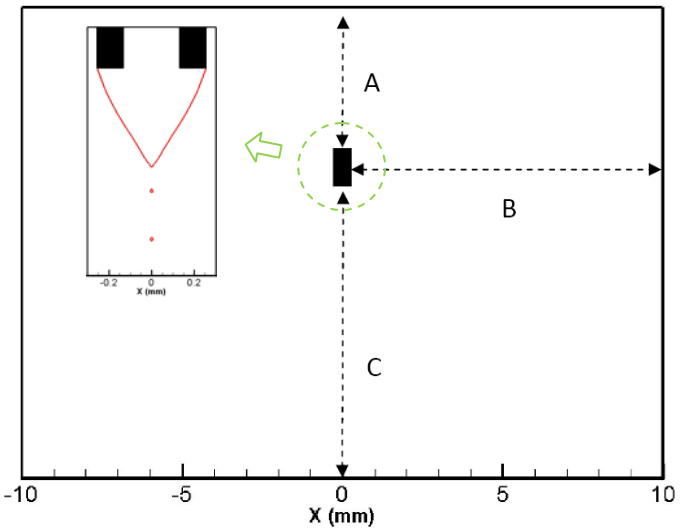

Figure 8: The zone defined by solid black color at the centre of the domain is the zone 1 in which the hydrodynamic and electrostatic equations are solved and the rest of the domain is treated as zone 2 in which just electrostatic equations are solved. Magnified view of the zone 1 is also shown in the figure.

Uniform structured mesh is used for zone 1. The size of the mesh is reported by specifying the number of cells lying in the outside radius of the capillary nozzle, this number is referred to as CPR which is abbreviated form of "cells per radius". Results from different CPR values are displayed in Figure 9. The CPR values used are 40, 60, 90 and 135 which are multiplied by 1.5 in each step to obtain a more refined mesh for the next step. According to Figure 9 mesh independency is achieved for CPR values greater than 60 so this value is used for the simulations in the rest of the paper.

Non-uniform structured mesh is used for zone 2. Number of cells in directions A, B and C is 45, 90 and 90 respectively. Mesh independency has been verified for this zone too. The grid used for zone 2 is shown in Figure 10.

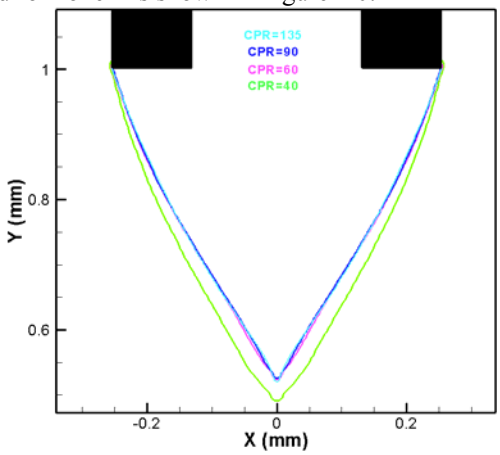

Figure 9: Steady state cone simulated using different mesh refinements. The results using CPR values greater than 40 are similar.

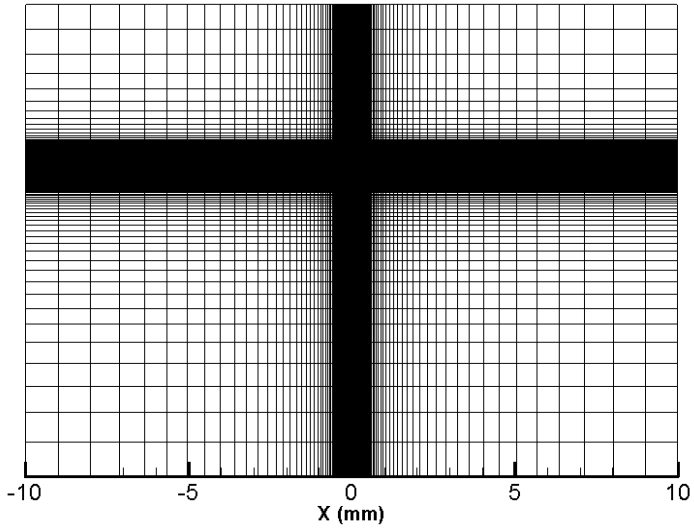

Figure 10: the grid used for numerical calculations.

Electrostatic atomization

The evolution of the formation of a cone-jet before atomization is illustrated in Figure 11. As shown in the second image, the jet is elongated due to the downwards electrostatic surface force. As the jet is elongated, the surface curvature increases at its tip and surface tension force overcomes electric force momentarily such that the jet tip returns upwards and becomes thicker. The procedure is repeated by electric force pulling the jet tip down until surface forces balance each other and jet becomes stable.

As an important point, it should be noted that, similar to the surface tension force, the sharper the curvature of the free surface, the greater the electrostatic force will be. This is because the electric field intensity has a greater value as a result of a greater electric potential gradient in the sharp edges (see Figure 13 as an example). Therefore, the electric force has the highest value at the tip of the liquid jet; this is the reason for the jet break up due to a large applied potential. As the jet becomes stable, the break-up takes place at the tip of the jet, i.e. fine droplets form and leave the liquid. The length scale of these droplets is very small compared to the jet diameter. Thus, it is necessary to use a very fine mesh to capture the exact characteristics of these separated droplets; this, in turn, increases the simulation time considerably. The behavior of the separated droplets, therefore, is not the focus of this study.

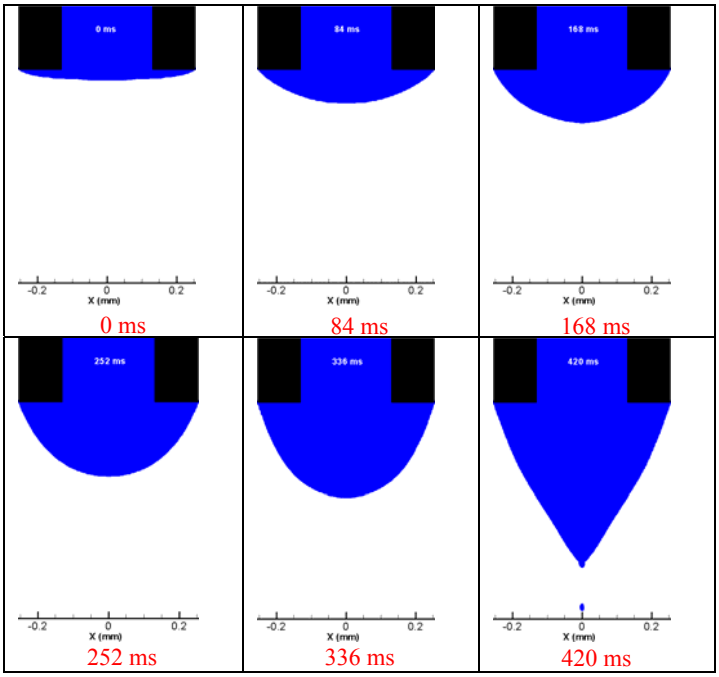

Figure 11: The evolution of a cone-jet formation. The time associated with each image is also shown in the figure. $Q = 5\ \mu L/min$, $\phi_0 = 2.8\ KV$

Figure 12 shows velocity flow field. According to this figure the velocity magnitude has its maximum at the cone tip which is a consequence of the high electrostatic force on this region, as mentioned before. In addition the vortex formed in the middle of cone is apparent in this figure. As explained above the liquid jet is pulled upwards being an effect of the surface tension force. Interaction of this upward flow with the downward flow at the nozzle outlet is the cause of this vortex.

As displayed in Figure 12 (Top) there is a vortex inside the cone which drives the flow entering the cone towards the

lateral surface, so the liquid flows on free surface and reaches the cone vertex. This causes the flow to accelerate and flow velocity on free surface gets considerably greater than the velocity of the flow inside the nozzle. therefore parasitic currents are negligible in this simulation.

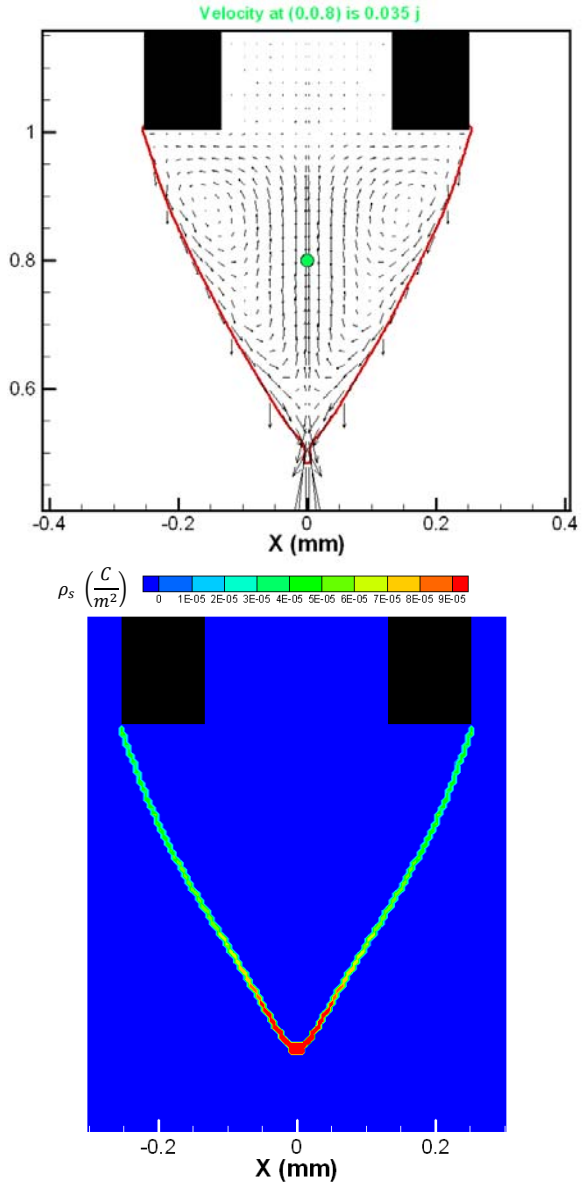

Figure 12: The velocity field (Top) and surface density (Bottom) of the electric charge at steady state.

The Surface charge density is also depicted in Figure 12. It is seen that the maximum density takes place at the tip of the jet. This effect was expected from Eq. (7) where the surface charge density is proportional to electric field intensity on the free surface. In other words, the electric field intensity, the charge density and the electric force, all reach their maximum value at the tip. Consequently the jet tip is pulled downwards. Since the nozzle flow rate is constant, as much as the jet elongates, its tip becomes more pointed. Therefore, a greater electrical force is exerted on the tip, thus its acceleration increases. On the other hand, a pointed tip has greater curvature which increases surface tension force upwards around the tip. Finally the opposite forces acting on the jet tip lead to the jet break up and a little part of the tip separates in the form of a droplet. The departure of a droplet decreases the curvature at the jet tip momentarily leading to jet backstroke. The same process is repeated establishing a spray operation. The determining effect of the surface tension on the break up phenomenon should be noticed here. Assume a liquid with no surface tension; in such a case, the velocity increase and the jet elongation at the tip leads to no break up and the jet diameter at the tip approaches zero.

In Figure 13 the electric potential distribution in the whole domain is illustrated. As observed, the equipotential lines get closer at the vicinity of the jet tip demonstrating that the potential gradient is high in this region.

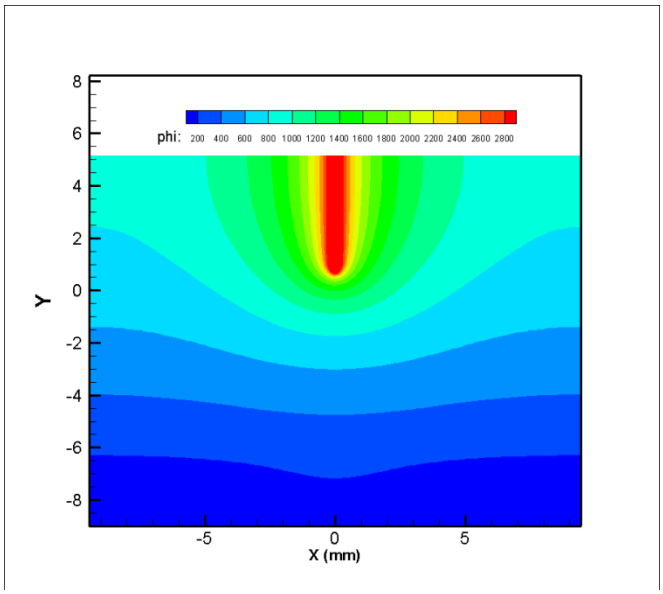

Figure 13: The electric potential distribution for the entire domain of computation.

CONCLUSIONS

In this study, a numerical model was developed to study the atomization of a liquid jet under an electrostatic field. The model was used to simulate the fluid flow distribution and free surface profile of a perfectly conductive liquid jet under the effect of an electric field. To validate the model, a case for which analytical results are available in the literature was considered. For a hemispherical solid placed on the lower plate of a charged capacitor, the electric field intensity values on the drop free surface was obtained from the numerical model and compared to those of the analytical data. The good agreement between the two results validated the model and its underlying assumptions.

The developed model has been utilized to simulate the electrospraying process and "Taylor cone" formation. Consecutive stages of cone formation are demonstrated. Velocity profile in steady state as well as electric charge density

and electric potential distribution in solution domain are numerically calculated and presented. Application of the model facilitates the simulation of different electrospraying modes and finding the conditions under which cone-jet mode occurs, all of these can be subjects for future works.

REFERENCES

[1] Jaworek, A. and Sobczyk, A.T., 2008, "Electrospraying Route to Nanotechnology: An Overview," Journal of Electrostatics, **66**, pp.197-219.

[2] Jaworek, A. and Krupa, A., 1999, "Classification of the Modes of EHD Spraying," Journal of Aerosol Science, **30**(7), pp. 873–893.

[3] Hartman, R. P. A., Borra, J. P., Brunner, D. J., Marijnissen, J. C. M., and Scarlett, B., 1999, "The Evolution Of Electrohydrodynamic Sprays Produced In The Cone-Jet Mode, A Physical Model," Journal of Electrostatics, **47**, pp. 143–170.

[4] Hartman, R. P. A., Brunner, D. J., Camelot, D. M. A., Marijnissen, J. C. M., and Scarlett, B., 1999, "Electrohydrodynamic Atomization In The Cone-Jet Mode Physical Modeling Of The Liquid Cone And Jet," Journal of Aerosol Science, **30**, pp. 823–849.

[5] Hartman, R. P. A., Brunner, D. J., Camelot, D. M. A., Marijnissen, J. C. M., and Scarlett, B., 2000, "Jet Break-Up In Electrohydrodynamic Atomization In The Cone-Jet Mode," Journal of Aerosol Science, **31**, pp. 65–95.

[6] Alfonso, M. and Ganan-Calvo, 1998, "The Surface Charge in Electrospraying: Its Nature and Its Universal Scaling Laws," Journal of Aerosol Science, **30**, pp. 863–879.

[7] FangYan, Farouka, B. and Ko, F., 2003, "Numerical Modelingof An Electrostatically Driven Liquid Meniscus In The Cone–Jet Mode," Journal of Aerosol Science, **34**, pp. 99-116.

[8] Zeng, J., Sobek, D., and Korsmeyer, T., "Electro-Hydrodynamic Modeling Of Electrospray Ionization: CAD For A Mfluidic Device – Mass Spectrometer Interface," Flow 3D Inc.

[9] Lastowa, O., and Balachandran, W., 2006, "Numerical Simulation of Electrohydrodynamic (EHD) Atomization," Journal of electrostatics, **64**, pp. 850-859.

[10] Jackson, J. D., 1998, *Classical electrodynamics*, John Wiley and sons.

[11] Melcher, J. R., 1981, *Continuum electromechanics*, The MIT press.

[12] Berry, S., 2008, "Electrowetting Phenomenon for Microsized Fluid Devices," PhD Thesis, Tufts University.

[13] Youngs D.L., 1982, "Time Dependent Multi Material Flow with Large Fluid Distortion," Numerical Methods for Fluid Dynamics, pp. 273-285.

[14] Brackbill J.U., Kothe D.B., and Zamach C., 1992, "A continuum method for modeling surface tension," Journal of Computational Physics, **100**, pp. 335-354.

[15] Bussmann, M., 2000, "A Three-Dimensional Model of an Impacting Droplet," Ph.D thesis, University of Toronto, Toronto.

[16] Jomaa, Z., and Macaskill, C., 2005, "The Embedded Finite Difference Method for the Poisson Equation In a Domain With an Irregular Boundary and Dirichlet Boundary Conditions". Journal of Computational Physics, **202**, pp. 488-506.

[17] Jeans, J., 1960, *Mathematical Theory of Electricity and Magnetism*. Cambridge University Press, Cambridge, UK.

[18] Bateni, A., Susnar, S. S., Amirfazli, A., and Neumann, A. W., 2004, "Development of A New Methodology to Study Drop Shape and Surface Tension in Electric Fields," Langmuir**, 20**, pp. 7589-7597.